1 **Selectivity enhancement for Ruthenium atomic layer deposition in sub-50 nm nanopatterns by**
2 **diffusion and size dependent reactivity**

3 *Jan-Willem J. Clerix, Esteban A. Marques, Job Soethoudt, Fabio Grillo, Geoffrey Pourtois, J.*
4 *Ruud Van Ommen, Annelies Delabie**

5 Jan-Willem J. Clerix, Esteban A. Marques, Dr. Job Soethoudt, Prof. Dr. Annelies Delabie
6 Department of Chemistry, KU Leuven, Celestijnenlaan 200F, 3001 Heverlee, Belgium
7 Imec, Kapeldreef 75, 3001 Heverlee, Belgium
8 *E-mail Annelies.Delabie@imec.be

9 Dr. Fabio Grillo
10 Department of Materials, ETH Zurich, Zurich, 8093, Switzerland

11 Dr. Geoffrey Pourtois
12 Imec, Kapeldreef 75, 3001 Heverlee, Belgium

13 Prof. Dr. J. Ruud Van Ommen
14 Department of Chemical Engineering, TU Delft, 2629 HZ Delft, The Netherlands

15 Keywords: area-selective deposition, diffusion, ruthenium, nanoelectronics, atomic layer
16 deposition

17 Area-selective deposition (ASD) is a promising bottom-up approach for fabricating
18 nanoelectronic devices. However, a challenge is to prevent undesired growth of nanoparticles
19 on the non-growth area. In this work, we use kinetic Monte Carlo (KMC) methods to
20 investigate the defectivity in Ruthenium ASD by (ethylbenzyl)(1-ethyl-1,4-
21 cyclohexadienyl)Ru/O_2 (EBECHRu) atomic layer deposition (ALD) in line-space nanopatterns
22 with different dimensions. Ru ASD is governed by adsorption as well as diffusion. The
23 defectivity depends on the pattern dimensions, as nanoparticles can diffuse and reach the
24 interface with the growth area where they aggregate. For linewidths of 50 nm and smaller, all
25 Ru adspecies are captured at the growth interface before growth by precursor adsorption is

confidential

26 catalysed. The synergetic effect of diffusion and size-dependent reactivity reduces defectivity
27 below 10^{10} Ru atoms cm^{-2} for at least 1000 ALD cycles. This is more than 1000 times lower
28 than for patterns with a linewidth of 200 nm and larger, where the Ru content decreases
29 significantly only near the interface with the growth surface. The predicted depletion zone is
30 confirmed by experiments in nanoscale line-space patterns. Overall, this mechanism results in
31 smaller and fewer Ru nanoparticles for smaller patterns, facilitating the development of
32 passivation-deposition-etch ASD processes for nanoelectronic device fabrication.

33 **1. Introduction**

34 The semiconductor industry continuously improves the performance and power consumption
35 of nano-electronic devices by decreasing device dimensions, by implementing new materials
36 and by introducing new device concepts and architectures. As a consequence, the device
37 fabrication processes by classic top-down lithography and patterning are becoming
38 increasingly complex and expensive.[1] Area-selective deposition (ASD) promises to simplify
39 and improve the fabrication processes.[2, 3] ASD aims to grow materials only where needed,
40 from the bottom up, by selective deposition on one surface area, the growth surface, while
41 preventing growth on another area, the non-growth surface. As such, nanopatterns can be
42 replicated or small features can be filled up from the bottom. ASD can simplify and improve
43 the fabrication process by reducing the number of steps, limit edge placement errors, and offer
44 a new patterning paradigm.[4, 5]

45 The selectivity of chemical vapor deposition (CVD) processes is known to rely on different
46 kinetics of the adsorption, desorption and diffusion processes on the growth and non-growth
47 surface area.[6] Fast adsorption and fast reactions on the growth surface lead to film growth.
48 Selective deposition occurs when adsorption on the non-growth surface is much slower, by
49 fluxes of intermediate species from the non-growth to growth area by surface and/or gas phase

confidential

50 diffusion, and/or by etch and desorption processes of intermediate species on the non-growth
51 surface. These kinetics in selective epitaxy by high temperature CVD are often process inherent
52 but can be improved by surface modification.[7-9] The roles of gas phase and surface diffusion
53 have long been known in selective epitaxial growth by CVD.[6, 7, 10-20] The resulting fluxes
54 reduce deposition on the non-growth surface and enhance the growth rate on the growth
55 surface. As a consequence, the growth rate and selectivity depend on the pattern dimensions
56 and geometry when the pattern dimensions are comparable or smaller than the characteristic
57 diffusion length.[6, 12, 21-23] For example, diffusion processes in selective Si epitaxy by $SiCl_4/H_2$
58 CVD at 1200 °C are characterized by diffusion lengths in the μm-range, at least partially driven
59 by the very high temperatures of these processes.[6, 24] The impact of surface diffusion and
60 aggregation was recently also demonstrated for Ru ASD by (carbonyl)(cyclohexadienyl)Ru/H_2
61 CVD at a much lower deposition temperature of 250°C, driven by high surface energy of Ru
62 and the low surface energy of the methyl-terminated SiO_2 non-growth surface.[12] The
63 experimental-theoretical study indicated an average diffusion length of 140 nm for Ru
64 adspecies on the methyl-terminated SiO_2 non-growth substrate. Indeed, diffusion-mediated Ru
65 ASD was observed in SiO_2-TiN line-space patterns with a critical dimension of 45 nm and
66 SiO_2 line height of 60 nm. Depletion of Ru nanoparticles near the interface with the growth
67 surface and a more than two times higher growth rate for ASD compared to CVD are consistent
68 with diffusion of Ru adspecies from the non-growth to the growth area, where they contribute
69 to Ru growth.[12, 25] Almost no Ru deposition was present on the SiO_2 sidewalls, indicating that
70 diffusion can be an ally in defect mitigation.

71 While the concept of diffusion mediated ASD is widely described for high temperature CVD,
72 only few papers discuss the role of diffusion in area-selective Atomic Layer Deposition (AS-
73 ALD) in nanopatterns at moderate temperatures.[13, 14, 26] The selectivity of AS-ALD has so far

confidential

74 mostly been established by tuning the adsorption and desorption processes, for example by
75 using organic blocking layers, self-assembled monolayers, small inhibitor molecules, and/or
76 by etching the nanoparticles that can grow on the non-growth area.[3, 27] Interestingly, few
77 studies of diffusion processes during ALD exist. For example, diffusion and aggregation
78 processes have been proposed for trimethyl(methylcyclopentadienyl)Pt/O_2 ALD of Pt
79 nanoparticles on SiO_2 and graphene and for (ethylbenzyl)(1-ethyl-1,4-cyclohexadienyl)Ru/O_2
80 (EBECHRu) ALD of Ru nanoparticles on organosilicate glass (OSG).[13, 28-31] While the role
81 of diffusion is known, the impact on selectivity is not observed yet. This could be related to the
82 lack of studies in patterns with nanoscale dimensions: high impact on selectivity is expected
83 especially in patterns with dimensions in the same order or magnitude as the diffusion length,
84 which is only 16 nm for Ru adspecies in the EBECHRu/O_2 Ru ALD process on OSG.[13, 19, 32]
85 Another interesting feature of this Ru ALD process is the size-dependent reactivity of Ru
86 nanoparticles. Ru nanoparticles that are too small to catalyze O_2 dissociation do not grow by
87 precursor adsorption, which intrinsically limits the nanoparticle growth. This phenomenon is
88 highly interesting in view of selectivity. However, this Ru AS-ALD process has not been
89 studied extensively in patterns with nanoscale dimensions, where diffusion and size dependent
90 reactivity may affect selectivity. In addition, these dimensions are highly relevant for ASD
91 applications in nanoelectronic device fabrication, where insight in the ASD mechanism, the
92 defect density, and defect sizes is important for the design of defect mitigation strategies (such
93 as periodic passivation and etching).[2, 3, 33-37]

94 Therefore, in this paper, we investigate the mechanism of Ru ASD to understand the impact of
95 adsorption and diffusion on defectivity and selectivity in nanoscale line patterns with line
96 widths between 20 and 200 nm. We quantify the density and size of Ru nanoparticles on an

confidential

97 area-restricted non-growth surface as a function of the line width through simulations. The
98 theoretical predictions are supported by experimental results for Ru ASD in nanoscale patterns.

99 **2. Results and discussion**

100 **2.1. Ru ALD growth mechanism on blanket substrates**

101 In order to study patterned SiO_2 surfaces through simulations, the growth mechanism on
102 blanket (non-patterned) surfaces should first be described. The growth mechanism of
103 EBECHRu/O_2 ALD on a blanket OSG was already determined in a previous study.[13]
104 However, the pristine OSG surface is not representative for ASD as the surface composition
105 changes from methyl-terminated OSG to hydroxyl-terminated SiO_2 during the patterning
106 processes, and restoration of the methyl-termination is required to enable Ru ASD by ALD,
107 for example by *N,N*-dimethylamino-trimethylsilane (DMA-TMS).[32, 38, 39] We therefore first
108 investigate the Ru ALD growth mechanism on blanket SiO_2 substrates passivated with DMA-
109 TMS (SiO_2-$OSi(CH_3)_3$). SiO_2 is an omnipresent material in nanoelectronics and is a typical
110 non-growth surface for many practical implementations of Ru ASD. Passivation of SiO_2 by
111 DMA-TMS is known to reduce precursor adsorption in many ALD processes.[32, 39, 40] DMA-
112 TMS exposure is compatible with back-end-of-line processing. In this study, we therefore
113 determine the simulation parameters of EBECHRu/O_2 ALD on the blanket SiO_2-$OSi(CH_3)_3$
114 substrates, based on previously published experimental growth curves.[32] These experiments
115 were conducted in identical experimental conditions as the preceding study on OSG by our
116 group, so that the impact of the surface can be investigated.[13] The growth curves are compared
117 in **Figure 2** and the experimental conditions are included in the Experimental Methods for
118 reference.

119 The fundamental processes in the kinetic Monte Carlo (KMC) model used to simulate Ru ALD
120 have been previously described by Soethoudt et al.[13] KMC methods allow simulation of the

confidential

121 most important processes in Ru ALD in the relevant spatial (100's of nanometers) and temporal
122 (multiple cycles) frames. The microscopic evolution of the system is determined by a limited
123 set of events with known probability. The model describes the evolution of the particle size
124 distribution (PSD, see Supplementary Information), total amount of Ru (Ru atom areal
125 density), nanoparticle number density, and surface coverage during EBECHRu/O_2 ALD on
126 dielectric substrates.[32, 41] We define the most important quantities for ALD on non-growth
127 surfaces as follows;

128 - The PSD is the normalized probability of finding a Ru nanoparticle of a given radius
129 on the non-growth area.
130 - The Ru atom areal density is the amount of Ru atoms per unit surface area (at cm^{-2}) of
131 the non-growth surface area.
132 - The Ru nanoparticle number density is the amount of Ru nanoparticles per unit surface
133 area (cm^{-2}) of the non-growth surface area.
134 - The coverage is the percentage of the non-growth area covered by Ru nanoparticles.
135 - The growth-per-cycle (GPC) is the amount of Ru atoms deposited per unit area and
136 cycle (at cm^{-2} cy^{-1}) on the non-growth area.
137 - The steady state GPC is the growth rate of Ru ALD on a blanket Ru substrate or on the
138 surface of a Ru nanoparticle (nm cy^{-1}).

139 The simulated substrate is a two-dimensional lattice with square sites with sides of 0.356 nm,
140 the diameter of a Ru atom. Ru adatoms are deposited on the uncovered part (i.e., not covered
141 by Ru particles) of the starting SiO_2-$OSi(CH_3)_3$ surface each cycle, parametrized as G_s (at nm^{-}
142 ^{2}). G_s was experimentally determined as the Ru atom areal density after 1 ALD cycle through
143 total X-ray fluorescence spectroscopy (TXRF), i.e. it is the GPC in the first Ru ALD cycle. 6.3

confidential

144 10^{-4} at nm^{-2} are instantaneously deposited on the free surface at the start of every simulated
145 cycle in a random spatial distribution.

146 On this surface, Ru adspecies are able to diffuse as described by the power law (**Equation 1**):

147 $$D_k = D_1 k^{-s} \quad (1)$$

148 Where D_k is the average diffusion coefficient of a particle of k atoms (nm^2 cy^{-1}), D_1 is the
149 average diffusion coefficient of a Ru adatom (nm^2 cy^{-1}) and s (-) is a factor that describes the
150 decrease in diffusion length with particle size. The adatoms and particles diffuse over the
151 surface and irreversibly aggregate with each other to form new hemispherical particles
152 composed of the combined number of atoms. An average diffusion length (nm cy^{-1}) of a particle
153 of k atoms can be defined as (**Equation 2, Figure 1**, right):

154 $$\lambda_k = \sqrt{D_k} \quad (2)$$

155 D_1 and s were determined by fitting the experimental PSD, Ru atom areal density, nanoparticle
156 number density and coverage through a previously published mean field model to experimental
157 data.[13, 28] The determined parameters correspond to Ru ALD at 325°C with a 5s EBECHRu,
158 5s N_2, 0.4s O_2, 3s N_2 cycle (see Experimental Methods). The diffusion parameters of a similar
159 Pt ALD process were shown to depend O_2-coreagent pulse length and substrate temperature;
160 however, these parameters are not investigated here.[11]

161 Collisions of Ru adatoms and/or nanoparticles lead to instantaneous, irreversible aggregation
162 due to the limited temperature (325°C) and high pair bond energy, also seen in the irreversible
163 integration of Ru nanoparticles in Ru films at the interface with the growth area.[12, 42, 43] The
164 Ru nanoparticles are hemispherical, with a height to radius ratio of 1, which was determined
165 by transmission electron microscopy (TEM, Supplementary Information). The surface area is
166 approximated as an hcp-truncated hexagonal bipyramid [1011]+[0001].[44, 45]

confidential

167 Diffusion of adatoms and nanoparticles on blanket substrates is described accurately by
168 applying periodic boundary conditions.[13] Species that diffuse across one of the sides of the
169 700 nm by 700 nm simulated substrate reappear on the opposite side. The simulations were
170 repeated until a total 10^7 nm^2 substrate area was simulated.

171 Only when a particle has grown through diffusion and aggregation to reach a critical diameter
172 (d_c) of 0.85 nm, it becomes catalytically active toward O_2 dissociation.[13, 46] This diameter
173 corresponds to particles of at least 12 atoms (Figure 1, left). The catalytic activity allows the
174 direct adsorption of Ru precursors on the Ru particle each cycle, which results in a constant
175 radial growth of 0.03 nm cy^{-1}, as determined to be the steady state GPC of Ru ALD on a Ru
176 surface in refs[13, 41]. To obtain a constant radial growth, the number of deposited atoms depends
177 on the surface area of the hemispherical hcp-truncated hexagonal bipyramid [1011]+[0001]
178 particle and is determined by the parameter G_p (at (surf. at)$^{-1}$). Therefore, 0.1261 Ru atoms are
179 deposited per surface atom of the nanoparticle ($> d_c$). Direct deposition on the particle is
180 characteristic of the Ru material and ALD process conditions and is independent of the
181 dielectric substrate type. In the simulations, particles grow instantaneously at the start of each
182 cycle.

183 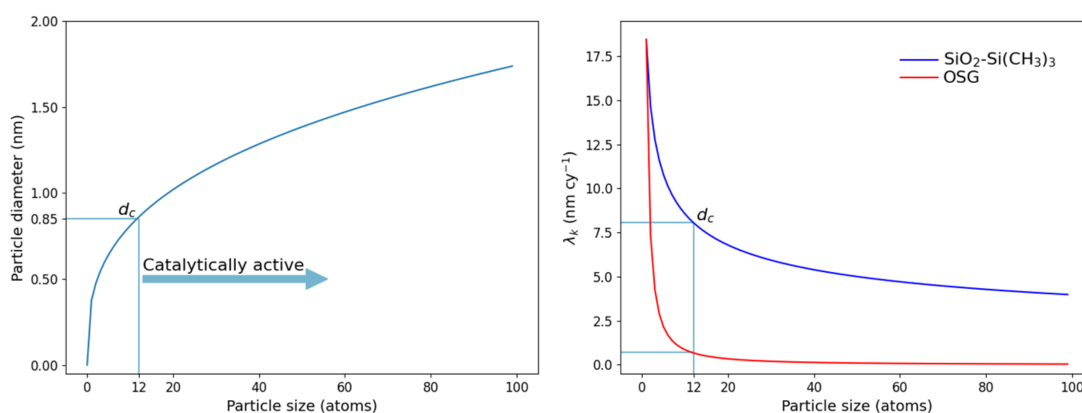

confidential

184 **Figure 1** Left: particle diameter (nm) as a function of particle size (atoms). Particles of at least 185 12 atoms have reached d_c and are catalytically active toward O_2 dissociation, i.e., they will 186 also grow through fast precursor adsorption on the particle itself. Right: λ_k (nm cy^{-1}) as a 187 function of particle size (atoms). At size 1, λ_k is the average diffusion length of an adatom. For 188 a Ru adatom on SiO_2-$OSi(CH_3)_3$ this is 18 nm cy^{-1} as determined in this study, on OSG, this is 189 16 nm cy^{-1} as determined previously.[13] The λ_k of Ru particles on SiO_2-$OSi(CH_3)_3$ is halved 190 by the time they reach the critical diameter (d_c); after which it reduces continuously at a slower 191 rate. On OSG, the size-dependence of λ_k is much more pronounced and particles at $d_c$are 192 effectively immobile.

193 The parameters that describe Ru ALD on SiO_2-$OSi(CH_3)_3$ are compared to those of OSG in 194 **Table 1**. Overall, we observe a less pronounced growth inhibition on SiO_2-$OSi(CH_3)_3$ than on 195 OSG in the experimental growth curves (Figure 2). TXRF shows a slightly higher deposition 196 rate on the surface (G_s) on SiO_2-$OSi(CH_3)_3$ than on OSG. One possible cause for the higher 197 deposition rate is the higher -OH group density on SiO_3-$OSi(CH)_3$ (0.4 nm^{-2}) compared to OSG 198 (< 0.1 nm^{-1}).[10, 24] The critical diameter (for catalysis of O_2 dissociation) and the deposition 199 rate on the Ru particles are independent of the substrate.

confidential

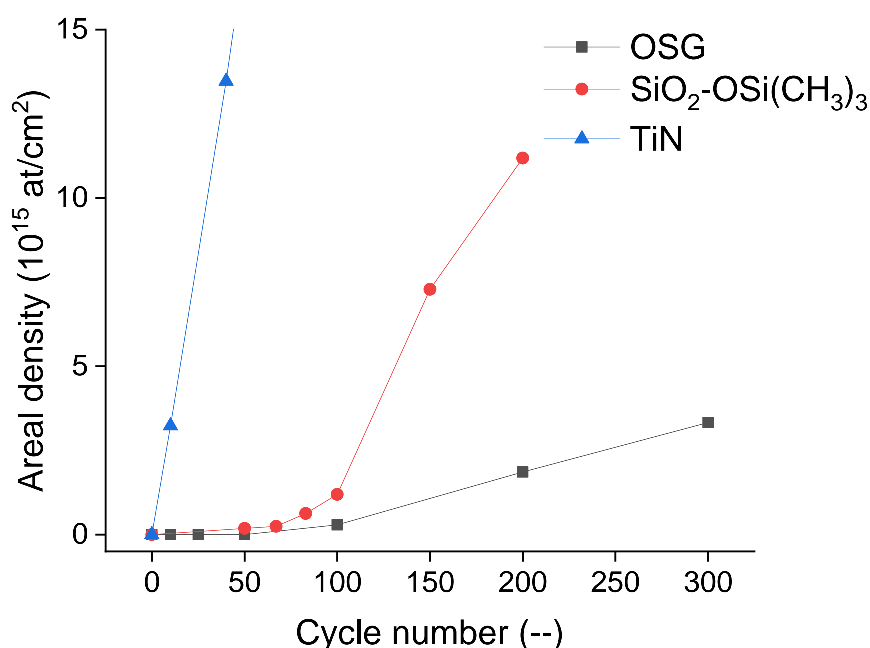

200

201 **Figure 2** Experimental growth curves of Ru ALD at 325 °C on OSG, SiO_2-$OSi(CH_3)_3$, and
202 TiN. Growth curve on SiO_2- $OSi(CH_3)_3$ obtained as discussed in the Experimental Methods.
203 Growth curves on OSG and TiN taken from ref[13, 38].

204 The different growth behavior of Ru ALD on the two substrates is also attributed to differences
205 in the diffusion kinetics. Adatom diffusion is slightly faster on the SiO_2-$OSi(CH_3)_3$ surface
206 (D_1), and particle diffusion is less size-dependent (s) than on OSG. A size dependence $s < 1$
207 on SiO_2-$OSi(CH_3)_3$ indicates that even large particles will continue to be mobile. Especially for
208 particles larger than d_c, λ_k reduces slower with particle size (Figure 1, right). On OSG,
209 diffusion and aggregation will only be of importance for adatoms and small clusters ($< d_c$).
210 On SiO_2-$OSi(CH_3)_3$, the greater mobility will result in the formation of larger particles than on
211 OSG. At the same time, the larger diffusion lengths of adatoms and nanoparticles will reduce
212 the nanoparticle number density. The larger diffusion lengths on SiO_2-$OSi(CH_3)_3$ might be
213 attributed to differences in surface composition and roughness. The surface roughness of SiO_2-

confidential

214 $OSi(CH_3)_3$ (RMS = 0.14 nm) is lower compared to OSG (0.79 nm), as determined by AFM

215 (see Supplementary Information).

216 **Table 1** Parameters for KMC simulations of Ru ALD on the OSG and SiO_2-$OSi(CH_3)_3$

217 surfaces.

218

219

	OSG	**SiO_2-$OSi(CH_3)_3$**
$\boldsymbol{G_s}$	1.5 10^{-4} at nm^{-2} cy^{-1}	6.3 10^{-4} at nm^{-2} cy^{-1}
$\boldsymbol{D_1}$	270 nm^2 cy^{-1}	340 nm^2 cy^{-1}
$\boldsymbol{s}$	8/3	2/3
$\boldsymbol{G_p}$	0.1261 at (surf. at.)$^{-1}$ cy^{-1}	
$\boldsymbol{d_c}$	0.85m	

confidential

220 **2.2. Ru ASD growth mechanism on 200 nm wide line patterns: model and experiment**

221 Ru ALD on SiO_2-$OSi(CH_3)_3$ nanopatterns is expected to behave differently than Ru ALD on
222 non-patterned substrates, as the surface diffusion and aggregation near the growth/non-growth
223 interface can affect the growth rate, density, and spatial distribution of Ru nanoparticles. In a
224 next step, we therefore simulate the growth behavior in area restricted non-growth surfaces.
225 These serve to approximate the experimental line-space patterns as described later in this paper
226 (**Figure 3**). The existing KMC code was therefore modified to describe deposition on the area
227 restricted non-growth area of heterogeneous substrates. Nanoparticle growth on the non-
228 growth surface is described in the same manner as for Ru ALD on the SiO_2-$OSi(CH_3)_3$ blanket
229 substrates. In this approximation, we therefore neglect the impact of minor changes in surface
230 composition that may occur due to the patterning processes. However, the impact of left and
231 right interfaces with a growth surface area are assumed to act as particle sinks: particles that
232 reach the interfaces are removed from the simulation to mimic irreversible aggregation and
233 incorporation into the growing Ru film on the growth surface (Figure 3). This has been shown
234 to be an appropriate assumption in other diffusion-mediated Ru ASD processes.[12] Periodic
235 boundary conditions are applied along the depth-direction. The linear Ru ALD growth on the
236 growth surface is not modeled explicitly. As such we model the impact of the restricted surface
237 area of the non-growth area and the proximity of interfaces with the growth area. As the
238 hypothetical Ru film is not explicitly incorporated, the possible overgrowth of Ru onto the non-
239 growth surface is not considered in the simulations. This is in keeping with the application of
240 ASD in a line-space pattern, where lateral overgrowth is not a concern. Note that in planar line
241 patterns lateral overgrowth might be possible and might be enhanced by diffusion from the
242 non-growth area.

confidential

243

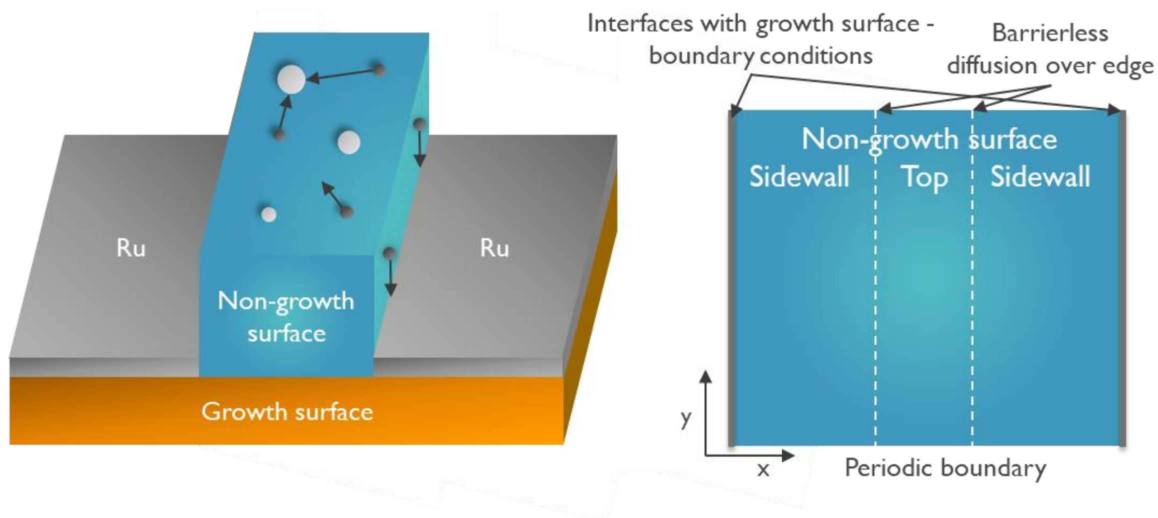

244

245 **Figure 3** Left: schematic of a three-dimensional line space pattern after ASD. Right: schematic
246 of the planar area-restricted approximation used in the KMC simulations.

247 Area-restricted substrates with widths between 20 and 200 nm were simulated, to investigate
248 the impact of the line width on the ASD mechanism. For the 200 nm wide area-restricted
249 substrate, the line width is an order of magnitude larger than the average diffusion length of a
250 Ru adatom (18 nm). The depth of the substrate unit cell was fixed at 700 nm. For each area-
251 restricted substrate, a total substrate area of over 10^7 nm^2 was simulated. These surfaces were
252 exposed to up to 167 cycles of Ru ALD. However, we will focus mainly on the range 50-100
253 cycles, as this corresponds to the thicknesses (2.5-5 nm) of interest for possible ASD
254 applications of the Ru ALD process.[38] For the smallest area-restricted substrates with widths
255 of 20 and 50 nm, up to 1000 cycles were simulated. The results of these simulations for 200
256 nm wide area-restricted substrate are compared to those for blankets in **Figure 4**.

257 As predicted, the Ru surface coverage, Ru atom areal density, and nanoparticle number density
258 for Ru ALD on the 200 nm area-restricted substrate are lower as compared to Ru ALD on
259 blanket substrates. The Ru nanoparticle number density is 35% lower on the area-restricted

confidential

260 substrate after 50 ALD cycles. The decreased surface coverage and Ru atom areal density are
261 a result of the reduced Ru nanoparticle number density. The Ru nanoparticle number density
262 decreases as Ru adatoms and nanoparticles diffuse and reach the interface where they
263 aggregate. Nanoparticle growth by aggregation is reduced due to the larger average distance
264 between the nanoparticles. As a direct result, growth by direct precursor adsorption is also
265 reduced as fewer nanoparticles reach a diameter that is larger than the critical size. Overall, the
266 area-restricted and blanket surfaces yield Ru nanoparticles with a similar particle size
267 distribution (PSD), which is a result of the same growth mechanism (Figure 4). Particles reach
268 roughly the same size, although the size of the largest nanoparticle is slightly reduced at all
269 cycle numbers.

270

confidential

271

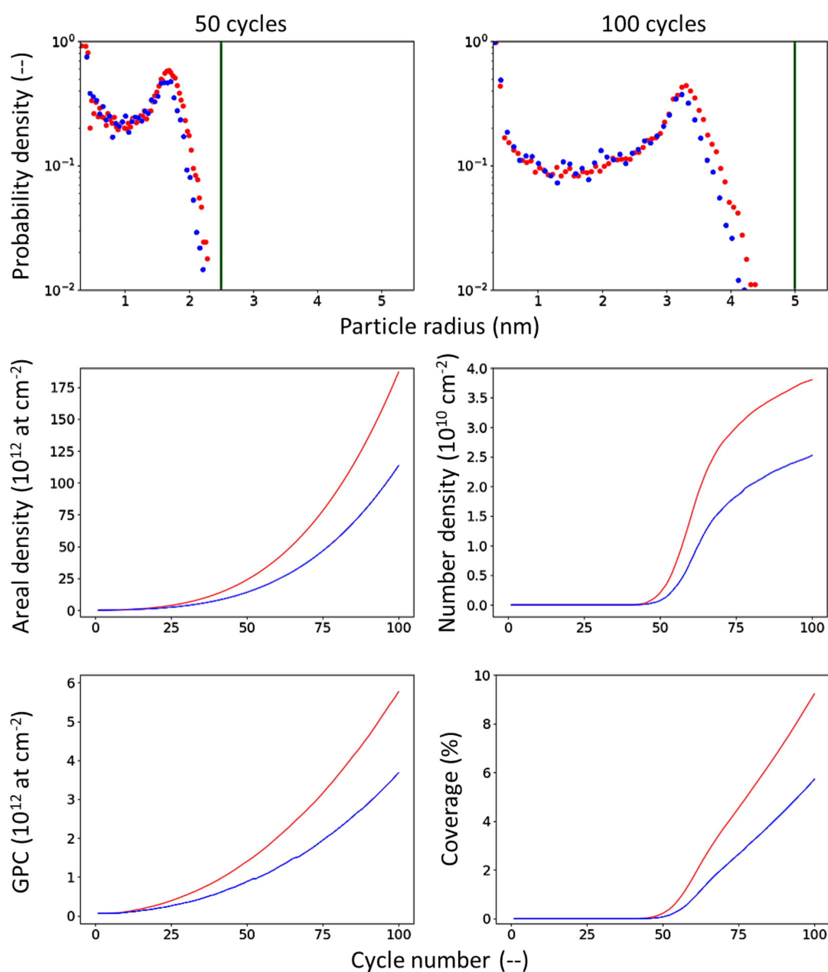

272 **Figure 4** Comparison of Ru ALD growth on blanket (red) and 200 nm-wide area-restricted
273 (blue) SiO_2-$OSi(CH_3)_3$ non-growth surfaces. Top: probability density of particle radii for a
274 given number of cycles. The green vertical line represents the thickness of an equivalent Ru
275 ALD film on a TiN growth surface. Middle: Ru atom areal density and nanoparticle number
276 density. Bottom: Ru ALD GPC, comprising deposition on both nanoparticles and the free
277 surface, and Ru coverage.

278 The diffusion of Ru adatoms and particles does not only impact the overall amount of deposited
279 Ru on the non-growth area, but it also affects the spatial distribution of the Ru adspecies
280 (**Figure 5**). We observe a much lower Ru nanoparticle number density close to the interfaces
281 with the growth area as compared to the center of the non-growth area. This is due to the

confidential

282 average diffusion length of Ru adatoms (18 nm), which is much smaller compared to the line
283 width (200 nm). The Ru atom areal and nanoparticle number densities therefore gradually
284 increase with increasing distance from interface and reach a steady value at a distance of 50
285 nm from the interface. Henceforth, we will refer to the zones on the non-growth area less than
286 50 nm from the interfaces as depletion zones. After 50 ALD cycles, the average nanoparticle
287 number density in the depletion zones is 57% lower compared to the density on blanket
288 substrates, while the Ru atom areal density is 65% lower. In the center of the 200 nm-wide
289 area-restricted substrate, at a distance of more than 50 nm from both interfaces with the growth
290 area, we find a constant nanoparticle number density. Still, the nanoparticle number density at
291 the center is 9% lower compared to blanket substrates, while the Ru atom areal density is 18%
292 lower.

293 The width of the depletion zone (50 nm) is mainly determined by the likelihood of an adatom
294 encountering another adatom, which decreases as the distance to the growth interface
295 decreases. For this reason, fewer large, immobile particles are formed in the depletion zone,
296 which in turn prevents the fast growth by direct precursor adsorption. This self-reinforcing
297 mechanism based on the size dependent reactivity of the Ru nanoparticles contributes to a
298 depletion zone extending 50 nm from the interface with the growth substrate, i.e., almost three
299 times the average diffusion length (18 nm).

confidential

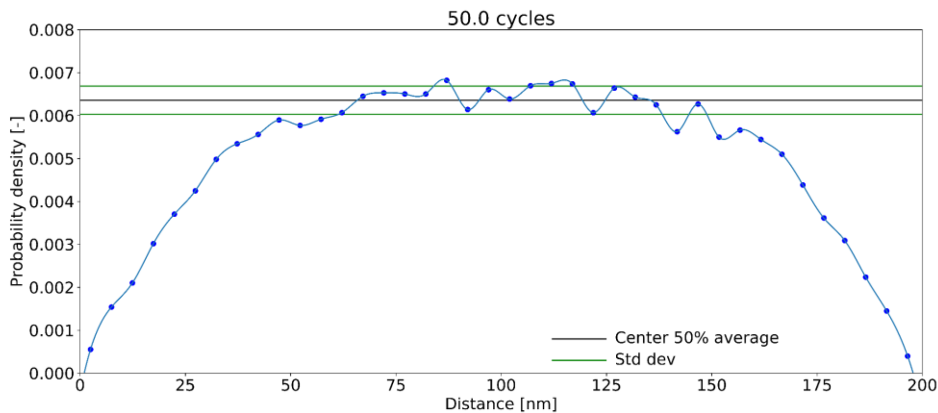

300

301 **Figure 5** Probability density of finding a Ru nanoparticle at a certain distance along the width
302 of 200 nm-wide area-restricted substrate after 50 Ru ALD cycles. The black line marks the
303 average probability of finding a particle in the center 50% of the area-restricted substrate (from
304 50 to 150 nm), the green lines are the standard deviation. These values serve as a guide to
305 distinguish between the center constant value and the depletion zones closer to the interface.
306 The blue line serves as a guide to the eye.

307 The depletion has limited impact on the particle size distributions, as most of the particles are
308 located in the center of the area-restricted substrate. As a result, the PSD is similar for Ru ALD
309 on the area-restricted and blanket substrates. The average particle radius is only slightly smaller
310 for 200 nm-wide area-restricted substrates compared to blanket substrates as shown by the PSD
311 (Figure 4, top). On the other hand, we find that the size of the largest nanoparticle is slightly
312 reduced at all cycle numbers. This indicates that the same mechanism that leads to depletion
313 extends throughout the 200 nm wide line: diffusion to and collection at the growth interface
314 reduces the nanoparticle number density of nanoparticles over the entire area-restricted
315 substrate. This reduces the likelihood of nanoparticle growth by aggregation, limits the size of
316 the nanoparticles and as such their reactivity towards precursor adsorption by the catalytic
317 effect.

confidential

318 To experimentally verify the existence of depletion zones in nanopatterns, 42 cycles of Ru
319 ALD were applied on SiO_2/TiN line-space patterns with a 90 nm repeating unit (pitch) (see
320 Experimental Methods). The patterns were treated with DMA-TMS before ALD, to obtain a
321 SiO_2-$OSi(CH_3)_3$ non-growth surface while TiN remains reactive.[32, 39] The spatial distribution
322 of Ru nanoparticles on the SiO_2 sidewalls was studied by scanning-tunneling electron
323 microscopy (STEM). Particle size distributions and coverages are extracted from the images
324 for three equally-sized bands on the sidewall (**Figure 6**).

325 The STEM results confirm that diffusion in Ru AS-ALD creates a depletion zone with lower
326 Ru nanoparticle coverage near the interface with the growth surface, as predicted. The band
327 near the interface with the growth area shows a shift of the particle size distribution to smaller
328 sizes than further away from the interface. The shifted particle size distribution near the
329 interface shows both a smaller average particle size and a 0.7 nm smaller largest particle, when
330 compared to the other bands. This finding corresponds well with the theoretical prediction of
331 reduced defectivity on area-restricted substrates close to the interface. Depletion toward the
332 interface with the TiN growth area is clearly visible in the Ru coverage. As predicted, diffusion
333 results in fewer and smaller particles near the interface. The extent of the depletion is smaller
334 than in the simulations, which predicted a 65% decrease in the total amount of Ru in the
335 depletion zone. This difference could be due to the patterning processes, which expose the
336 sidewall to CF_4/CHF_3 etchants and an O_2 plasma strip. These treatments could modify surface
337 chemistry and morphology. The role of the top surface and the three-dimensional topography
338 are also not captured in the simulations.

confidential

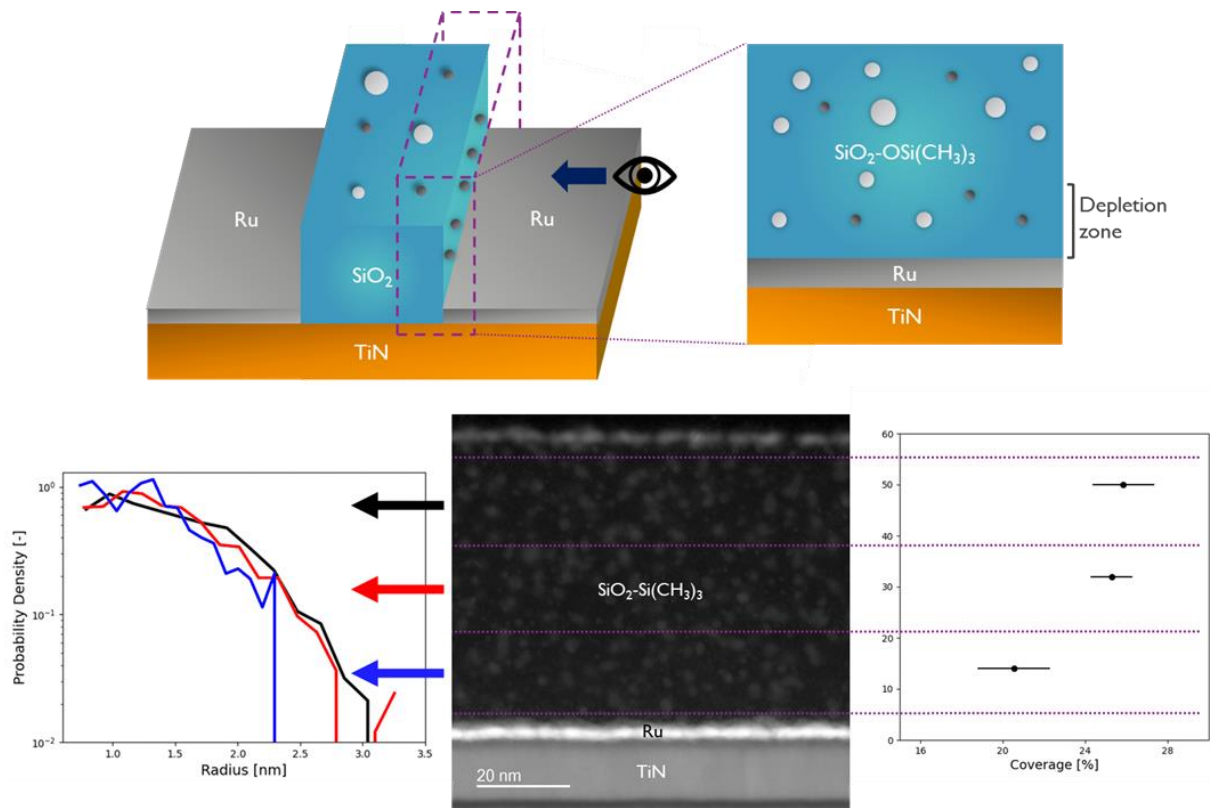

339

340 **Figure 6** Top: schematic showing the outline of the line-space pattern. Dark blue dashed lines
341 mark the cut of the STEM lamella as prepared by focused ion beam (FIB). The eye symbol
342 marks the imaging direction perpendicular to the line. A schematic of the resulting view from
343 the STEM imaging direction perpendicular to the lamella, is also provided. Bottom center:
344 STEM image of a sidewall after 42 Ru ALD cycles with Ru nanoparticles on the SiO_2-
345 $OSi(CH_3)_3$ non-growth area and a closed Ru film of 2.2 nm thick on the TiN growth area.
346 Bottom left: particle size distribution for three bands on the sidewall (marked by color). Bottom
347 right: Average coverage with standard deviation for three bands on the sidewall.

348 **2.3. Impact of line width (20-200 nm) on Ru ASD growth mechanism**

349 Reducing the area-restricted substrate width drastically decreases the Ru atom areal density on
350 the non-growth surface (**Figure 7**). As the two growth interfaces come closer, there is a higher
351 probability of collection of particles at the interface with the growth area. Interestingly, we find
352 a sharp decline in the Ru atom areal density at a line width of 50 nm: reducing the line width

confidential

353 from 200 to 50 nm results in a thousand-fold decrease in the Ru atom areal density and in much
354 smaller particles. This thousand-fold decrease in Ru atom areal density is related to a synergetic
355 effect of diffusion and size-dependent reactivity of the Ru nanoparticles during ALD. For line
356 widths of 50 nm and smaller, the Ru nanoparticles are captured at the growth interface before
357 they can aggregate and reach the critical size where growth by precursor adsorption and
358 catalytic reactions starts to occur.

359 Indeed, also the size of the Ru particles dramatically decreases with decreasing area-restricted
360 substrate width for line widths of 50 nm and smaller due to the synergetic effect of diffusion
361 and size-dependent reactivity. To investigate the size of the largest particles, we collect the 95th
362 percentile particle radii, as using the 95th percentile will reduce the impact of outliers (**Figure**
363 **8**). Even for 100 ALD cycles, 95% of the particles stay smaller than 0.3 nm in radius. This
364 means that these particles do not grow by adsorption, as the minimum radius needed for
365 catalytic activity is 0.43 nm (Figure 8). Interestingly, the size of these particles does not
366 increase as a function of the number of ALD cycles for up to at least 1000 cycles (which would
367 correspond to 50 nm Ru on a blanket TiN surface). This confirms that Ru nanoparticles are
368 effectively captured at the interface with the growth area before their growth by means of
369 adsorption is catalyzed, and the defect capture mechanism persists even during extensive ALD
370 cycles.

371 Despite the drastic impact of diffusion in the non-growth area, we expect limited impact on the
372 steady state GPC on the growth area. The low adsorption rate of the EBECHRu precursor on
373 the non-growth area (6.3 10^{-4} Ru at nm^{-2} cy^{-1}) in combination with the prevented adsorption of
374 EBECHRu on the Ru nanoparticles due to the lack of the catalytic activity result in a small flux
375 of Ru atoms from the non-growth to growth area. Previously, the steady state GPC on the TiN
376 growth area was shown to be much faster at 3.7 Ru at nm^{-2} cy^{-1}.[41] We therefore expect that

confidential

377 the diffusion processes will not significantly affect the growth rate on the growth area in line
378 patterns. This is confirmed by cross-section TEM of the line-space pattern after ALD
379 (Supplementary Information). The cross-section demonstrates that the Ru film thickness is
380 uniform over the growth area, with no measurable thickness increase near the interface with
381 the non-growth surface. This is in contrast to the diffusion-mediated ASD by
382 (carbonyl)(cyclohexadienyl)Ru/H_2 CVD, where the precursor adsorption rates on the growth
383 and non-growth areas are similar and the average diffusion length (140 nm) is an order of
384 magnitude larger.[12] In that case, a large flux of Ru adspecies from the non-growth area to the
385 growth area resulted in enhanced growth rates for ASD versus blanket CVD.[25]

386 Finally, we discuss the impact on selectivity. The common definition of selectivity is given in
387 **Equation 3**:[27]

388 $$s = \frac{\theta_G - \theta_{NG}}{\theta_G + \theta_{NG}} \quad (3)$$

389 With s the selectivity, θ_G the Ru atom areal density on the growth area and θ_{NG} the Ru atom
390 areal density on the non-growth area. Only a qualitative prediction of enhanced selectivity can
391 be made as the deposition on TiN was not studied by the same methods as deposition on SiO_2-
392 $OSi(CH_3)_3$. Ru ALD on a TiN growth surface occurs fast with a steady state GPC of 0.05 nm
393 cy^{-1} and is known to be independent of growth area dimensions of at least 36 nm and larger.[38,
394 41] We consider that the Ru atom areal density (θ_G) on the TiN growth surface does not depend
395 on the growth area line width, and the more-than-linear dependence of the Ru atom areal
396 density (θ_{NG}) on the SiO_2-$OSi(CH_3)_3$ non-growth surface width. Together, these two
397 dependencies will result in a selectivity increase with decreasing dimensions of the area-
398 restricted non-growth area. However, this prediction relies on the assumption of no pattern
399 dependence of deposition on the growth area.

confidential

400

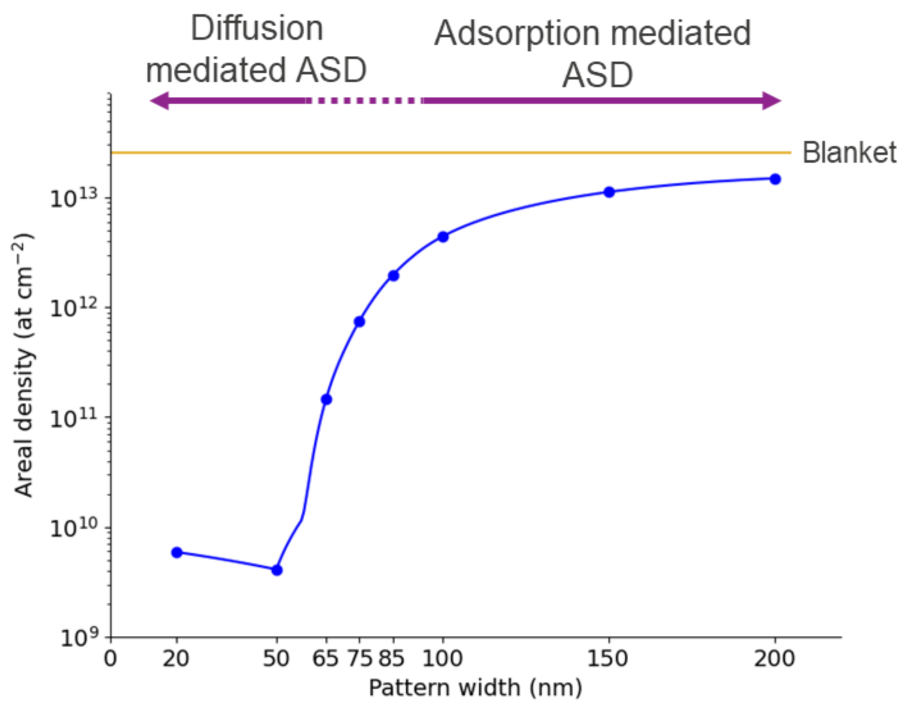

401 **Figure 7** Ru atom areal density after 50 cycles of Ru ALD as a function of area-restricted

402 substrate width. The green line represents the Ru atom areal density on a blanket substrate. The

403 continuous blue line serves as a guide to the eye.

404

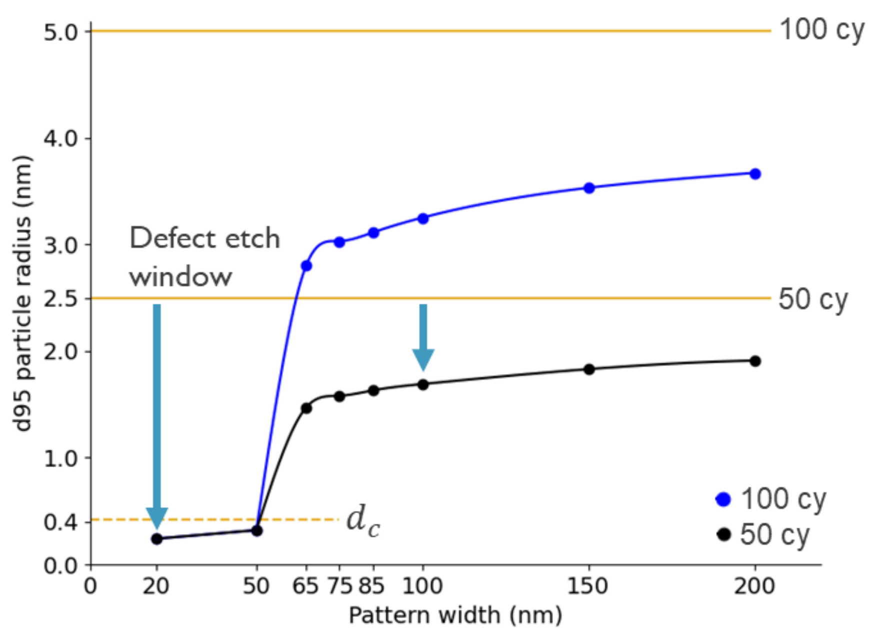

confidential

405 **Figure 8** For area-restricted substrate widths below 50 nm, diffusion of Ru adspecies to the
406 growth surface keeps particles smaller than the critical radius, which drastically reduces
407 deposition on the non-growth surface. The 95th percentile Ru particle radius is plotted as a
408 function of area-restricted substrate width for 50 and 100 cycles Ru ALD. The orange lines
409 represent the thickness of an equivalent Ru film on TiN, a typical growth surface. The critical
410 radius is marked by a dashed line. The defect etch is illustrated for 20 and 100 nm wide area-
411 restricted substrates after 50 cycles. The continuous blue and black lines serve as guides to the
412 eye.

413 **2.4. ASD growth regimes and defect mitigation**

414 Our findings predict two ASD growth regimes for Ru ASD by ALD, depending on the line
415 width (Figure 7). For a line width of the non-growth area of 65 nm and larger, ASD is
416 dominated by the differences in the adsorption kinetics on the growth and non-growth surface
417 area. In this regime, additional passivation and/or defect mitigation are necessary as Ru
418 nanoparticles grow in the non-growth area, as demonstrated here and previously.[33, 38] The
419 maximum size of the particles and how it compares to the Ru film thickness on the growth area
420 is important when assessing isotropic, non-selective defect etching as defect mitigation
421 approach. A defect-free ASD condition can be obtained if all particles, including the largest
422 ones, are fully etched, while a closed ASD-grown film remains on the growth area. A simplified
423 metric to predict the ASD defect etch window is the difference between the Ru film thickness
424 and the maximum island height, assuming that films and particles are etched at the same rate.
425 The maximum island height is indicated by the 95th percentile particle radius (Figure 8For a
426 200 nm-wide area-restricted substrate, the defect etch window is similar to that for blanket
427 substrates, i.e., 1.3 nm after 100 cycles. Cycles of passivation/ALD/etch can be used to extend
428 the Ru thickness while maintaining good selectivity.

confidential

429 An even more positive perspective is provided for Ru ALD when the line widths of the non-
430 growth area are 50 nm and smaller. In this case, the ASD is governed by adsorption as well as
431 diffusion and nanoparticle growth is inhibited by the size-dependent reactivity. Defectivity is
432 largely suppressed by diffusion to the growth area and any remaining Ru nanoparticles are so
433 small that they are not susceptible to precursor adsorption. As these particles remain smaller
434 than the critical diameter of 0.85 nm even for extensive ALD cycles, a single corrective etch
435 after passivation and ALD can be effective. The calculations therefore predict that a high
436 selectivity (see ref.[3, 27]) can be maintained for much higher Ru thicknesses, up to at least 50
437 nm. While for adsorption based ASD with a line width of 200 nm, the defect etch window is
438 small after 100 ALD cycles (corresponding to 5 nm Ru on the growth surface), the window
439 widens to 4.7 nm for diffusion mediated ASD with a line width of 20 nm. This diffusion
440 mediated ASD regime provides us with a positive outlook for the removal of the minor amount
441 of Ru defects by brief etching.

442 3. Conclusion

443 Our combined theoretical-experimental study of Ru ASD by ALD reveals a synergetic effect
444 of surface diffusion and size-dependent reactivity of Ru nanoparticles in nanoscale patterns
445 with dimensions $\leq$ 50 nm. This mechanism limits defectivity during Ru ASD, as Ru
446 nanoparticles are effectively captured at the growth surface interface before growth by
447 adsorption is catalyzed. Ru nanoparticles that exist in very low concentrations on the non-
448 growth surface area are so small that effective removal by a one-step non-selective, isotropic
449 defect etch processes should be straightforward. Our predictions of low defectivity at small
450 pattern sizes show great promise for application in nano-electronic device fabrication.
451 However, our work also illustrates the need for studies of ASD mechanisms in nanoscale
452 patterns with small dimensions, as different phenomena may occur due to the close proximity

confidential

453 of the growth and non-growth surface. Surface and/or gas phase diffusion during ASD by ALD
454 and CVD in nanoscale patterns merits further investigation. The KMC simulations were found
455 to be a valuable tool in that respect. Still, the predictive ability of the KMC simulations could
456 be further improved by considering growth as well as non-growth area, topography and surface
457 modifications inherent to patterning. It would also be interesting to investigate whether
458 diffusion in nanopatterns might be enhanced by tuning coreagent exposure and substrate
459 temperature.

460 **4. Experimental Methods**

461 Ru ASD is achieved by selectively passivating the SiO_2 non-growth surface with DMA-TMS.
462 The DMA-TMS treatment renders the surface methyl-terminated.[47] The EBECHRu/O_2
463 island-like ALD growth rate will then be reduced significantly due to inhibited precursor
464 adsorption.[32, 39] The DMA-TMS does not react extensively with metal and metal nitride
465 substrates, such as TiN, and does not noticeably reduce the growth rate of EBECHRu/O_2 ALD
466 on TiN (0.05 nm cy^{-1}). In a pattern defined by a SiO_2 non-growth surface area and a TiN growth
467 surface area, ASD of Ru metal on metal nitride is then enabled.[38, 40]

468 Experimental growth curves on blanket substrates were performed on 300 mm Si[100] wafers.
469 75 nm hydrophilic SiO_2 (2.5 -OH groups per nm^2) was grown by plasma-enhanced ALD in an
470 ASM Eagle 12 reactor at 75 °C. The DMA-TMS treatment was performed by static exposure
471 in a TEL Tactras system with showerhead-type reactor. The wafers were kept at 5 Torr N_2 at
472 250 °C for 10 minutes to ensure clean surfaces. The N_2 is then evacuated and subsequently
473 replaced by 500 sccm DMA-TMS and 350 sccm N_2 to a total pressure of 5 Torr. The wafers
474 were exposed to this ambient for 5 minutes each. EBECHRu/O_2 ALD was performed in an
475 ASM Pulsar 3000 reactor on a Polygon8300 platform.[41] An ALD cycle consisted of 5 s
476 EBECHRu, 5 s N_2, 0.4 s O_2, 3 s N_2. The ALD process was shown to be self-limiting on TiN

confidential

477 and SiO_2.[41] Note that the self-limiting character on SiO_2-$OSi(CH_3)_3$ was not investigated. As
478 such, the extend of growth inhibition and nanoparticle growth could depend on the precursor
479 dose and on the total cycle time.

480 Line-space patterns with 45 nm critical dimension were created on 300 mm Si[100] wafers by
481 physical vapor deposition (PVD) of 15 nm TiN in a an AMAT Endura tool. On top of the TiN,
482 75 nm plasma-enhanced ALD SiO_2 was grown in an ASM Eagle 12 reactor at 75 °C. The
483 lithography stack on SiO_2 was comprised of 100 nm spin-on-carbon (SOC), 30 nm spin-on-
484 glass (SOG), 29 nm antireflective coating and 105 nm photoresist, which was exposed in a 193
485 nm immersion ASML Twinscan NXT:1950i. The pattern was transferred into the SiO_2 layer
486 until exposure of the TiN layer by CF_4/CHF_3 etch, followed by an O_2 plasma strip in a TEL
487 Tactras tool. Finally, the patterns were cleaned to remove possible F contamination. DMA-
488 TMS and ALD processing were identical to discussed above.

489 The Ru atom areal density after 1 ALD cycle was determined by TXRF in a Rigaku TXRF300
490 tool with a 24 keV beam. Ru atom areal density for other cycles was determined by Rutherford
491 backscattering spectrometry (RBS) with a 1.523 MeV He^+-ion beam. Samples were imaged by
492 SEM in a FEI Helios 460 microscope or by STEM in a FEI Tecnai F30 ST microscope. PSDs
493 and nanoparticle number densities were measured on the obtained images in ImageJ by
494 extracting particle areas and converting those to radii by assuming circular particle shapes.
495 Surface roughness was determined by AFM with a Bruker Dimension Icon PT tool.

496 **Conflict of interest**

497 The authors declare no conflict of interest.

498 **Acknowledgements**

499 J. J. C. is SB PhD fellow at FWO (1SB4319N).

confidential

ToC:

Area-selective deposition is a novel bottom-up approach in nanoelectronics fabrication. We show through a combined experimental-theoretical approach how decreasing pattern sizes benefit selectivity and reduce defectivity in Ru area-selective atomic layer deposition. Going from 200 nm-wide to ≤ 50 nm-wide patterns, defectivity is reduced thousandfold.

J. J. Clerix, E. A. Marques, J. Soethoudt, F. Grillo, G. Pourtois, J. R. Van Ommen, A. Delabie*

Selectivity enhancement for Ruthenium atomic layer deposition in sub-50 nm nanopatterns by diffusion and size dependent reactivity

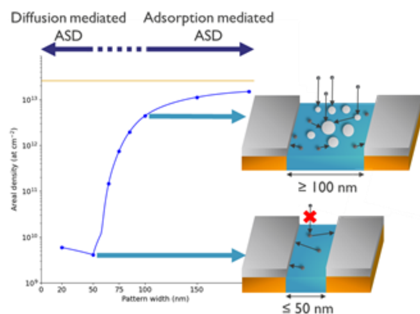

[1] M. M. Waldrop, *Nature* **2016,** *530* (7589), 144-147.

[2] A. J. M. Mackus, A. A. Bol, W. M. M. Kessels, *Nanoscale* **2014,** *6* (19), 10941-10960.

[3] A. J. M. Mackus, M. J. M. Merkx, W. M. M. Kessels, *Chemistry of Materials* **2019,** *31* (1), 2-12.

[4] R. Clark, K. Tapily, K. H. Yu, T. Hakamata, S. Consiglio, D. O'Meara, C. Wajda, J. Smith, G. Leusink, *APL materials* **2018,** *6* (5), 058203-058203-12.

[5] H. S. Suh, A. Delabie, S. Armini, *Semiconductor Digest* **2020,** *2*, 14-19.

[6] J. O. Carlsson, *Critical Reviews in Solid State and Materials Sciences* **1990,** *16* (3), 161-212.

[7] M. R. Goulding, *Journal De Physique Iv* **1991,** *1* (C2), 745-778.

confidential

520 [8] U. Jansson, J. O. Carlsson, *Journal of vacuum science & technology. A, Vacuum, surfaces,*
521 *and films* **1988,** *6* (3), 1733-1735.
522 [9] J. T. Fitch, *Journal of the Electrochemical Society* **1994,** *141* (4), 1046-1055.
523 [10] F. Grillo, TU Delft, Delft, 2018.
524 [11] F. Grillo, J. A. Moulijn, M. T. Kreutzer, J. R. van Ommen, *Catalysis Today* **2018,** *316*,
525 51-61.
526 [12] F. Grillo, J. Soethoudt, E. A. Marques, L. de Martin, K. Van Dongen, J. R. Van Ommen,
527 A. Delabie, *Chemistry of Materials* **2020,** *32*, 12.
528 [13] J. Soethoudt, F. Grillo, E. A. Marques, J. R. van Ommen, Y. Tomczak, L. Nyns, S. Van
529 Elshocht, A. Delabie, *Advanced materials interfaces* **2018,** *5* (24), 1800870-n/a.
530 [14] N. E. Richey, C. de Paula, S. F. Bent, *J Chem Phys* **2020,** *152* (4), 040902.
531 [15] J. Dendooven, S. P. Sree, K. De Keyser, D. Deduytsche, J. A. Martens, K. F. Ludwig, C.
532 Detavernier, *Journal of Physical Chemistry C* **2011,** *115* (14), 6605-6610.
533 [16] W. L. Gladfelter, *Chemistry of Materials* **1993,** *5*, 17.
534 [17] B. Korgel, R. F. Hicks, *Journal of crystal growth* **1995,** *151* (1), 204-212.
535 [18] Z. Zhang, M. G. Lagally, *Science (American Association for the Advancement of Science)*
536 **1997,** *276* (5311), 377.
537 [19] S. M. Gates, *Chem. Rev* **1996,** *96* (4), 1519-1532.
538 [20] J. O. Carlsson, *Vacuum* **1990,** *41* (4), 1077-1080.
539 [21] M. Bartek, P. T. Gennissen, P. J. French, R. F. Wolffenbuttel, *IEEE*: 1995; Vol. 1, pp 91-
540 94.
541 [22] X. Wang, J. Hartmann, M. Mandl, M. Sadat Mohajerani, H.-H. Wehmann, M. Strassburg,
542 A. Waag, *Journal of applied physics* **2014,** *115* (16), 163104.
543 [23] S. Jiang, C. Merckling, W. Guo, N. Waldron, M. Caymax, W. Vandervorst, M. Seefeldt,
544 M. Heyns, *Journal of Crystal Growth* **2014,** *391*, 59-63.

confidential

545 [24] B. D. Joyce, J. A. Baldrey, *Nature* **1962,** *195*, 2.

546 [25] A. Delabie, AVS ALD/ALE 2020 Tutorial: 2020; p 42.

547 [26] P. Klement, D. Anders, L. Gümbel, M. Bastianello, F. Michel, J. R. Schörmann, M. T.
548 Elm, C. Heiliger, S. Chatterjee, *ACS Appl. Mater. Interfaces* **2021,** *13* (16), 19398-19405.

549 [27] G. N. Parsons, R. D. Clark, *Chemistry of Materials* **2020,** *32* (12), 4920-4953.

550 [28] F. Grillo, H. V. Bui, J. A. Moulijn, M. T. Kreutzer, J. R. van Ommen, *Journal of Physical*
551 *Chemistry Letters* **2017,** *8* (5), 975-983.

552 [29] A. J. M. Mackus, M. J. Weber, N. F. W. Thissen, D. Garcia-Alonso, R. H. J. Vervuurt, S.
553 Assali, A. A. Bol, M. A. Verheijen, W. M. M. Kessels, *Nanotechnology* **2016,** *27* (3).

554 [30] J. Dendooven, R. K. Ramachanan, E. Solano, M. Kurttepeli, L. Geerts, G. Heremans, J.
555 Ronge, M. M. Minjauw, T. Dobbelaere, K. Devloo-Casier, J. A. Martens, A. Vantomme, S.
556 Bals, G. Portale, A. Coati, C. Detavernier, *Nat Commun* **2017,** *8* (1), 1074-1074.

557 [31] F. Grillo, H. Van Bui, D. La Zara, A. A. I. Aarnink, A. Y. Kovalgin, P. Kooyman, M. T.
558 Kreutzer, J. R. van Ommen, *Small* **2018,** *14* (23), 1800765.

559 [32] J. Soethoudt, Y. Tomczak, B. Meynaerts, B. T. Chan, A. Delabie, *Journal of Physical*
560 *Chemistry C* **2020,** *124* (13), 7163-7173.

561 [33] M. F. J. Vos, S. N. Chopra, M. A. Verheijen, J. G. Ekerdt, S. Agarwal, W. M. M. Kessels,
562 A. J. M. Mackus, *Chemistry of Materials* **2019,** *31* (11), 3878-3882.

563 [34] R. Vallat, R. Gassilloud, B. Eychenne, C. Vallee, *Journal of Vacuum Science &*
564 *Technology A* **2017,** *35* (1).

565 [35] S. K. Song, H. Saare, G. N. Parsons, *Chemistry of Materials* **2019,** *31* (13), 4793-4804.

566 [36] S. M. George, Y. Lee, *Acs Nano* **2016,** *10* (5), 4889-4894.

567 [37] G. N. Parsons, *Abstracts of Papers of the American Chemical Society* **2018,** *255*.

568 [38] J. Soethoudt, H. Hody, V. Spampinato, A. Franquet, B. Briggs, B. T. Chan, A. Delabie,
569 *Advanced Materials Interfaces* **2019,** *6* (20).

confidential

570 [39] J. Soethoudt, S. Crahaij, T. Conard, A. Delabie, *J. Mater. Chem. C* **2019,** *7* (38), 11911-
571 11918.
572 [40] R. Khan, B. Shong, B. G. Ko, J. K. Lee, H. Lee, J. Y. Park, I. K. Oh, S. S. Raya, H. M.
573 Hong, K. B. Chung, E. J. Luber, Y. S. Kim, C. H. Lee, W. H. Kim, H. B. R. Lee, *Chemistry of*
574 *Materials* **2018,** *30* (21), 7603-7610.
575 [41] M. Popovici, B. Groven, K. Marcoen, Q. M. Phung, S. Dutta, J. Swerts, J. Meersschaut,
576 J. A. van den Berg, A. Franquet, A. Moussa, K. Vanstreels, P. Lagrain, H. Bender, M. Jurczak,
577 S. Van Elshocht, A. Delabie, C. Adelmann, *Chemistry of Materials* **2017,** *29* (11), 4654-4666.
578 [42] C. Ratsch, A. Zangwill, P. Milauer, D. D. Vvedensky, *Phys Rev Lett* **1994,** *72* (20), 3194-
579 3197.
580 [43] C. Ratsch, J. A. Venables, *Journal of vacuum science & technology. A, Vacuum, surfaces,*
581 *and films* **2003,** *21* (5), S96-S109.
582 [44] E. S.Dana, *A Text-Book of Mineralogy*, Ford, W. E., Ed. John Wiley & Sons: New York,
583 1922; pp 94-98.
584 [45] R. Van Hardeveld, F. Hartog, *Surface science* **1969,** *15* (2), 189-230.
585 [46] J. Hämäläinen, M. Ritala, M. Leskelä, *Chem. Mater* **2014,** *26* (1), 786-801.
586 [47] J. J. Fripiat, J. Uytterhoeven, U. Schobinger, H. Deuel, *Helvetica Chimica Acta* **1960,** *23*,
587 7.
588

confidential